Non-Newtonian behaviour of hydrolysed polyacrylamide in strong elongational flows: a transient network approach

J. A. Odell, A. J. Müller and A. Keller
H. H. Wills Physics Laboratory, University of Bristol, Tyndall Avenue, Bristol BS8 1TL, UK
(Received 28 October 1987; revised 15 December 1987; accepted 18 December 1987)

In this paper we report a new technique that links molecular behaviour and macrorheology in idealized elongational flow systems. The effective elongational viscosity of aqueous solutions of hydrolysed polyacrylamide (widely used and studied in applied hydrodynamics) is determined and correlated with the various stages of chain stretching and transient network formation. Beyond a critical strain rate, strong non-Newtonian dilatant effects are observed. These are unmistakably due to the existence of transient networks, which arise as a consequence of entanglements becoming mechanically effective at timescales shorter than the disentanglement time. We report strong parallels between observations in our idealized experiments and dilatant effects commonly observed in other flow systems that contain appreciable elongational components. These effects had been previously generally attributed to the viscosity enhancement due to the stretching of isolated molecules. On the basis of our observations, which include the coil–stretch transition, we are forced to reinterpret such effects as also due to the development of transient entanglement networks.

(Keywords: extensional flow; non-Newtonian effects; viscosity; polyacrylamide; solution)

INTRODUCTION

Polymer solutions in flows of a predominantly rotational character (such as simple shear or couette flow) typically demonstrate a shear-thinning behaviour. In contrast to this, extremely dramatic dilatant effects have often been observed in flows that possess a predominantly elongational character. Such flows may be realized in practical situations: constrictions in pipes, flow through filters, valves and porous media, and in any flow possessing turbulence or vorticity.

These works have mostly been concerned with 'macrorheology' in complex non-ideal flow systems. Conversely in this laboratory we have recently developed techniques using near-ideal extensional flow systems to examine the effects of the flow field on molecular orientation and the subsequent perturbation of the flow field by the molecules.

In this paper our approach combines results on a molecular scale with those of macrorheology and leads us to present a new interpretation of many non-Newtonian effects. We begin with brief reviews of such effects and of our idealized elongational flow experiments. This background, though somewhat lengthy, is essential to the discussion and reinterpretation to be presented subsequently.

Review of non-Newtonian behaviour in extensional flows

In 1967 Dauben and Menzie[1] and Marshall and Metzner[2] examined the flow of apparently dilute solutions of poly(ethylene oxide) (PEO) and hydrolysed polyacrylamide (HPAA) through porous beds of glass beads. They reported an anomalous large increase in flow resistance as the flow rate was increased whilst remaining in the laminar region. *Figure 1* (after ref. 1) illustrates the effect. Beyond a critical flow rate (characteristic of the polymer species, molecular weight and solvent quality), the flow resistance increases markedly compared to pure solvent.

James and McLaren[3] suggested that the thickening in porous media flow was due to the extensional nature of pore entry flow. They suggested that the persistently extending nature of such flows could produce considerable stretching of the random-coil molecules, resulting in a dramatic increase in elongational viscosity.

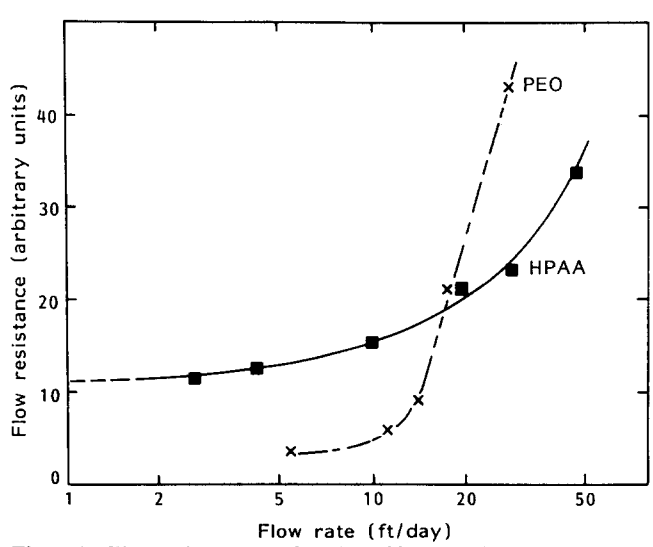

Figure 1 Flow resistance as a function of flow rate for 0.05% polymer solutions in 0.5 M NaCl in sandstone. After ref. 1. Flow resistance is here a normalized pressure drop. A Newtonian liquid would have a value of flow resistance independent of flow rate. (*Figures 1–4*, see refs. 1, 13 and 15)

Presented at the Polymer Physics Group Conference 'Physical Aspects of Polymer Science', Reading, 9–11 September 1987

0032-3861/88/071179-12$03.00

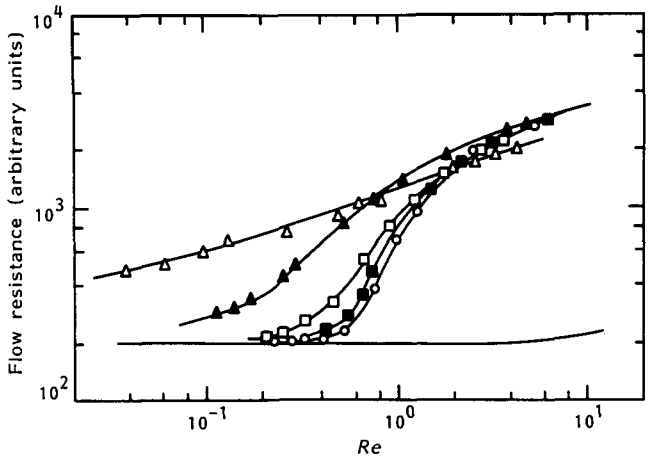

Figure 2 Influence of the ionic strength of the solvent, I_s (NaCl addition), on the flow resistance for solutions of HPAA (30.5% hydrolysis, $\bar{M}_v = 8.7 \times 10^6$, $c = 0.05\%$): △, $I_s = 0$ NaCl; ▲, $I_s = 0.05$ NaCl; □, $I_s = 0.20$ NaCl; ■, $I_s = 0.5$ NaCl; ○, $I_s = 2.00$ NaCl; ———, Newtonian fluid. After ref. 13

The condition required for coil–stretch transition to occur, as described by de Gennes[4] and Hinch[5], is that the strain rate should exceed a critical value, of the order of the reciprocal of the longest (lowest-order) relaxation time (τ) of the molecule. James and McLaren stated that the relevant relaxation time for PEO was the Rouse free-draining relaxation time. That the coil–stretch transition should produce a considerable increase in elongational viscosity is an expectation of the finitely extensible non-linear elastic (FENE) dumbbell models of Bird *et al.*[6–8] and others[9].

Ouibrahim *et al.*[10] in 1980 found dilational flow in three distinct flow situations which each involve an extensional component: capillary tube flow, orifice flow and pitot tube flow. They examined extensively hydrolysed polyacrylamide (HPAA) and found that the dilatant effect was greatly reduced in the presence of excess salt. This was attributed to the salt ions screening the charges on the polyelectrolytic HPAA causing the contraction of the highly expanded molecule.

Chauveteau *et al.*[11,12] have examined the flow of PEO and HPAA through the extensional flow produced in severe constrictions. They concluded that a coil–stretch transition was responsible for the dilatant behaviour observed, and that the critical shear rate required was of the order of 10 times the reciprocal of the Rouse relaxation time.

Perhaps the most extensive studies have been those of Haas and coworkers[13–15]. In a series of papers they have explored the critical dilatant behaviour on flow through porous media. These papers have further pursued the hypothesis that the phenomenon is primarily due to a coil–stretch transition beyond a critical deformation rate. They attempt a semiquantitative description based upon the dependence of the lowest-order relaxation time of the random coil upon polymer type, molecular weight, solvent quality and ionic environment.

Figure 2 illustrates the pronounced effect of the presence of counterions in HPAA. In pure water as a solvent, the flow resistance enhancement occurs at a very low flow rate. As the ionic strength is increased, the strain rate at which the dramatic enhancement in flow resistance occurs is markedly increased until beyond about 0.5 M no further effect occurs. The magnitude of the effect, however, remains approximately constant. It should be noted that the shear viscosity is greatly reduced by the increase in ionic strength. This effect is attributed to a progressive collapse of the HPAA coils due to counterion screening, resulting in a reduction in the conformational relaxation time and a consequent increase in the strain rate required to produce a coil–stretch transition.

Haas *et al.* report further that as their solutions approach the theta state they observe a more sharply critical transition with a shorter apparent relaxation time, which they ascribe to the Zimm relaxation time in the limit of hydrodynamic screening. *Figure 3* shows the flow resistance as a function of Reynolds number for a range of concentrations; they identify the condition $c^*[\eta] = 0.07$ as the boundary between the dilute and semi-dilute regions.

During flow in the dilatant region, Haas *et al.* observe accompanying degradation of the molecules, and associated reduction in the degree of viscosity enhancement (*Figure 4*). Typically they find that such degradation is not restricted to the high-molecular-

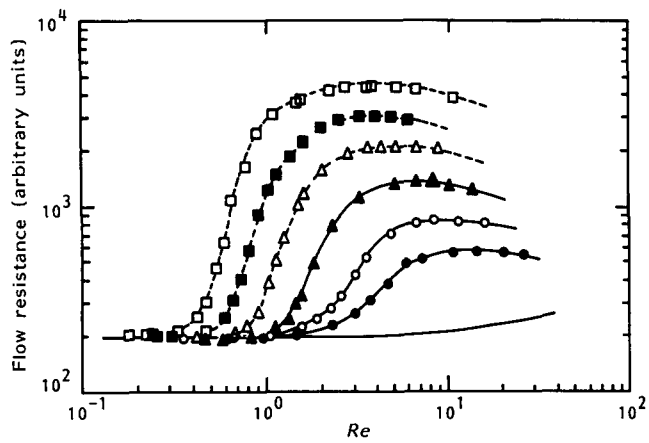

Figure 3 Flow resistance *versus* Reynolds number as a function of polymer concentration for solutions of PAA in 0.5 M NaCl ($\bar{M}_w \approx 18 \times 10^6$): □, 100 ppm; ■, 50 ppm; △, 25 ppm; ▲, 12 ppm; ○, 6 ppm; ●, 3 ppm. The full curve without points refers to the behaviour of a Newtonian fluid. After ref. 15

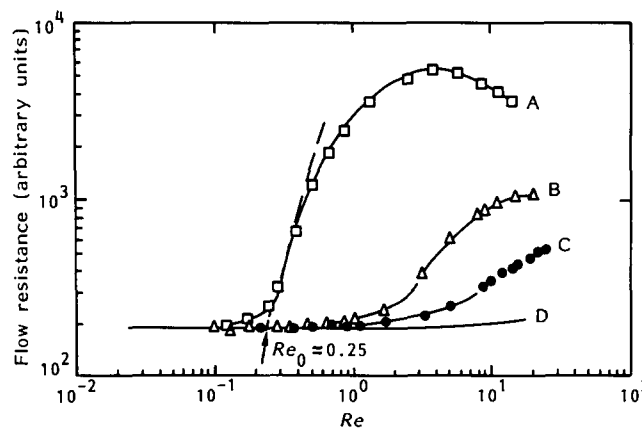

Figure 4 Flow resistance *versus* Reynolds number for a PAA copolymer of ultra-high molecular weight ($\bar{M}_w \simeq 27 \times 10^6$) in 0.5 M NaCl: A, first run; B, second run after forcing the solution through the porous medium at $Re = 15$; C, third run after forcing the solution through at $Re = 20$; D, Newtonian fluid. The onset Reynolds number where the non-Newtonian effect sets in (Re_0) is indicated for curve A. After ref. 15

weight components but occurs across a broad range of molecular weights for which the extension condition is satisfied.

More recently, papers on the subject by other authors have appeared which associate some of the extensional flow dilatant effect with aggregation and entanglements in the solution[16,17].

Background to extensional flow experiments

The background to our idealized extensional flow experiments has been reviewed in ref. 18 and is only briefly mentioned here for self-contained reading.

Our elongational flow techniques enable us to extend virtually fully polymer chains in solution, either in isolation or in overlapping conditions[18]. As stated earlier, isolated flexible long chains can be stretched in strong extensional flow fields provided that the extensional component of the velocity gradient dominates over the rotational component[19], and that the strain rate ($\dot{\varepsilon}$) exceeds a critical value ($\dot{\varepsilon}_c$) of the order of $1/\tau$. A number of experiments have been performed on dilute polymer solutions using strong extensional flow fields which have successfully corroborated the criticality of the coil–stretch transition [20–22].

Controlled strain rates in well characterized uniaxial extensional flow fields can be achieved by opposed jets[18] where the solution is sucked simultaneously into two jets that face each other with a small separation; such a system approximates pure hyperbolic flow.

It is characteristic of this flow field that it contains a point of zero velocity, i.e. a stagnation point, at its centre of symmetry. *Figure 5a* shows a schematic of the flow field incorporating a stagnation point O. The experimental flow field is shown in *Figure 5b*, where it is visualized by light scattered at 90° from tracer particles. In this paper, we concentrate on the opposed jets although other devices producing uniaxial and planar extension can be used[18].

Chain extension is usually monitored by observing the birefringence arising from the chain orientation between crossed polars. When dilute solutions are tested, the occurrence of the molecular extension at $\dot{\varepsilon}_c$ is signalled by the sudden appearance of a narrow birefringent line along the central outflow axis (as in *Figure 6a*). The narrowness of this birefringent line is due to the requirement that the deformed molecule must accumulate a large *strain* before it becomes highly birefringent. Such strains can only be realized by fluid elements that pass sufficiently close to the stagnation point; the molecules contained within those fluid elements will be resident in a high $\dot{\varepsilon}$ regime for a time interval sufficient to allow the uncoiling process to take place[23]. These experiments have been performed in dilute solutions of high-molecular-weight closely monodisperse atactic polystyrene (aPS)[20–25] and poly(ethylene oxide)[22,25]. They have enabled the direct assessment of τ for the isolated molecule, the evaluation of which has many practical and theoretical ramifications for polymer science[27,28].

The transient network in semi-dilute solutions

As the concentration is increased, the chains begin to interact and the extension behaviour is affected. Our technique provides a sensitive tool to identify the stage where the initially isolated molecules will begin to stretch out cooperatively[25]. As $\dot{\varepsilon}$ is increased in a semi-dilute solution, the appearance of a birefringent line at $\dot{\varepsilon}_c$ can still be observed as in *Figure 6a*. The only difference from the dilute case is a linear increase in τ with concentration, that is, now τ is proportional to the *solution* viscosity. This, together with the persistence of localization, means that the chains can still be extended as if in isolation provided they are given enough time. However, when $\dot{\varepsilon}$ is increased beyond $\dot{\varepsilon}_c$, new effects set in above a sharply defined concentration, to be denoted c_n^+. (Here the subscript 'n' relates to network effects; for details see ref. 29.)

The first observation with increasing strain rate is that the sharply localized line progressively broadens. This is followed by the appearance of a dark central line at $\dot{\varepsilon}_p$. This corresponds to the onset of the formation of a birefringent 'pipe' with a 'hollow' (i.e. non-birefringent) interior. Such a pipe is shown in *Figure 6b* for aPS. Photon-correlation velocimetry has revealed that the interior of the pipe corresponds to a reduced local flow velocity, It is postulated that the broadened chain-extended regions 'screen' the flow within, so that the flow velocity, and hence the extensional strain rate, drops below criticality ($\dot{\varepsilon}_c$) within the central zone (see ref. 29). For further increase in $\dot{\varepsilon}$, more complex strain patterns develop[29,30] until ultimately, beyond a third critical strain rate ($\dot{\varepsilon}_n$), the whole system becomes unstable and the final and most dramatic effect appears. This effect, which we term 'flare' is shown in *Figure 6c* also for aPS. Its characteristics are: (a) delocalization of the birefringence, which can occupy the whole volume between the jets, spread into them and spill over and beyond the entry side of the jet system; (b) the birefringence is highly unstable; (c) the flow field shows a breakdown of its cylindrically symmetric nature, indicating a flow instability that could not be associated with inertial turbulence[29].

In previous works this flare phenomenon has been interpreted as due to the formation of a transient network of entangled molecules. As the timescale of the experiment becomes shorter (as strain rate is increased—the timescale is of the order of $1/\dot{\varepsilon}$), the chains no longer have sufficient time to disentangle before extending. The solution then responds as a transient network and long-range orientation occurs, coupled with flow instability due to the inability of the network to comply with the (in principle) infinite strains in stagnation point flow. We interpret ($1/\dot{\varepsilon}_n$) as the effective disentanglement time of the network.

That this phenomenon is due to interchain effects is evidenced by its criticality with concentration: no effect is observed below c_n^+, at any available strain rate. The value of c_n^+ is, however, 10–50 times lower than the range of conventionally calculated c^* [25,30] based upon close packing of coils of radius R_g[31]. The real overlap criterion is more subtle than this and the Gaussian distributions of segment densities of coils overlap at much lower concentrations; then, whether the overlapping coils 'see' each other or disentangle depends upon the timescale of the experiment.

Extensional viscometry

The dramatic effects associated with the formation of transient networks have a correspondingly pronounced influence on the macroscopic flow behaviour. In order to measure these effects we developed a method of recording the pressure drop across the jets (flow resistance) as the

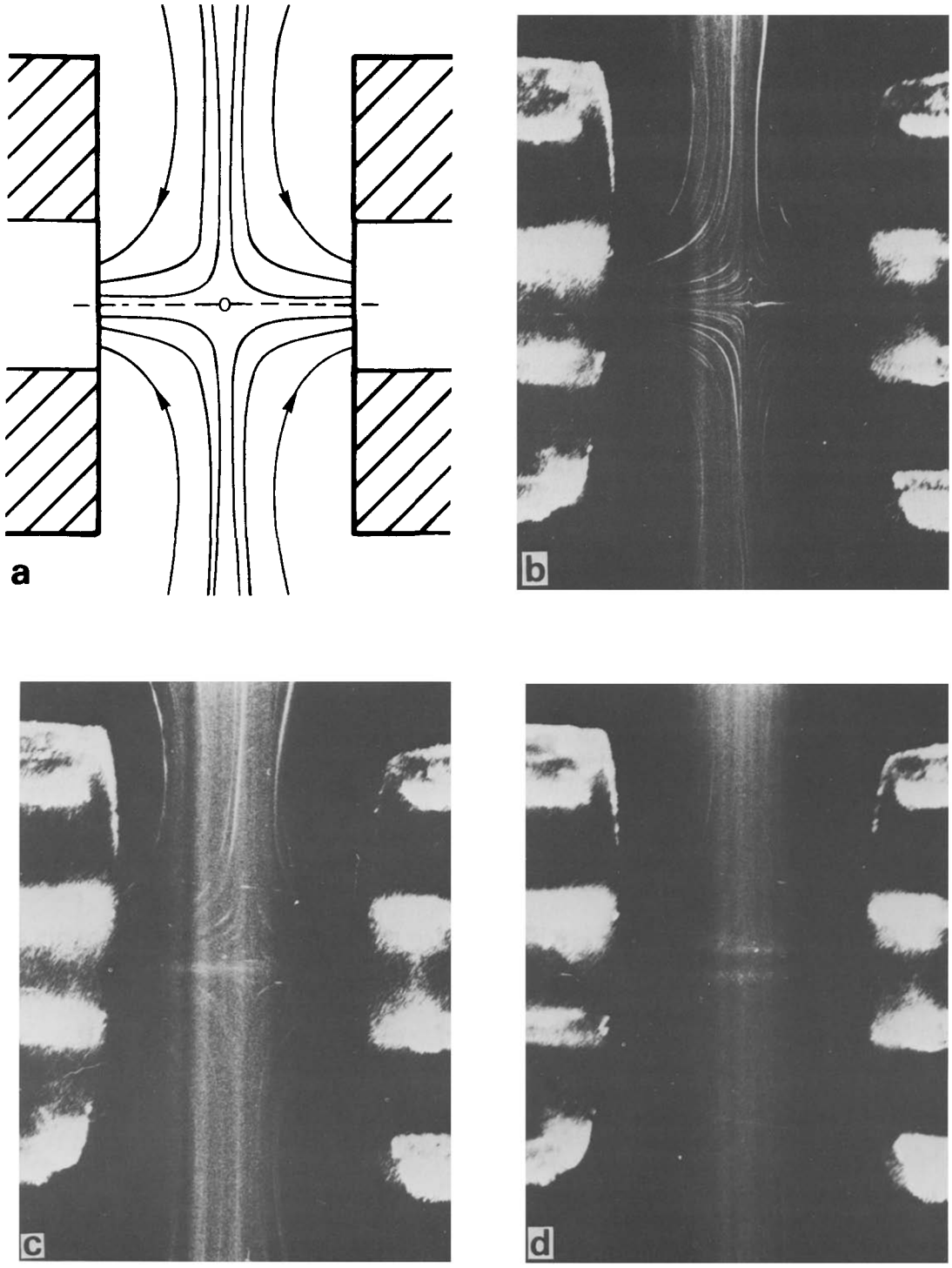

Figure 5 (a) The opposed jets. The polymer solution is sucked into the jets along the symmetry axis. O represents the stagnation point in the centre of the flow field. (b) The flow field visualized by light scattered at 90° from tracer particles: 0.25% Aldrich HPAA in 0.5 M NaCl solution ($\bar{M}_w > 5 \times 10^6$), $\dot{\varepsilon} \approx 50\,s^{-1}$ ($\dot{\varepsilon} < \dot{\varepsilon}_c$). (c) Light scattering effect observed at 90°. A line can be seen along the symmetry axis of the jets. The same solution as *Figure 5b* but $\dot{\varepsilon} \approx 295\,s^{-1}$ ($\dot{\varepsilon} > \dot{\varepsilon}_c$). (d) Light scattering effect observed at 90°. A 'pipe' can be seen along the symmetry axis of the jets. The same solution as in *Figure 5b* but $\dot{\varepsilon} \approx 540\,s^{-1}$ ($\dot{\varepsilon} > \dot{\varepsilon}_p$)

strain rate is increased[29,30]. Measuring the flow resistance, which closely relates to that measured in pore and capillary flow, whilst simultaneously observing the strain patterns arising from the birefringence of the stretched-out chains, has proved to be a very powerful technique[29].

This technique can be used to correlate directly the molecular behaviour and the rheology of the flowing solutions. Furthermore, it yields information about the degradation of the flowing solutions and has revealed that the flare state produces irreversible drops in elongational viscosity attributable to degradation; this causes a progressive increase in $\dot{\varepsilon}_n$ on subsequent re-runs[29]. Therefore, we decided to apply our technique to polymer solutions (i.e. high-molecular-weight hydrolysed polyacrylamides in brine) as widely used in pore and capillary flow experiments. We think we are in a position to determine, by observing the flow-induced birefringence,

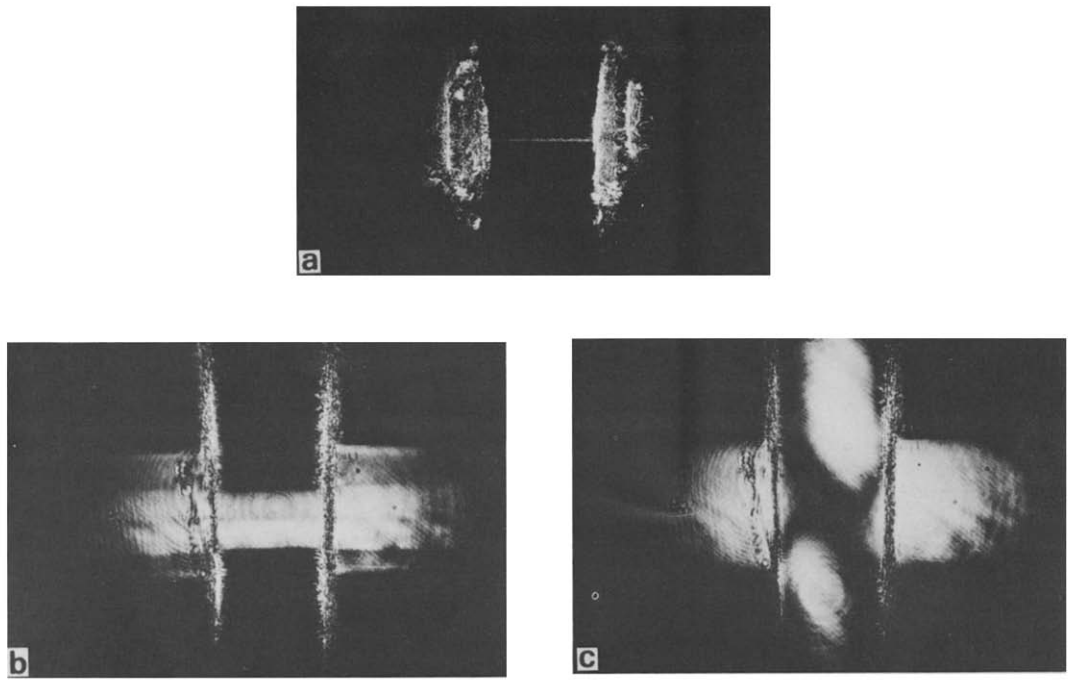

Figure 6 (a) A birefringent line between the jets for a 0.02% solution of aPS in decalin, $\bar{M}_w = 8 \times 10^6$ ($\dot{\varepsilon} > \dot{\varepsilon}_c$). (b) A birefringent pipe between the jets for a 0.3% solution of aPS in decalin ($\dot{\varepsilon} > \dot{\varepsilon}_p$). (c) A birefringent flare between the jets for the same solution as *Figure 6b* but at $\dot{\varepsilon} > \dot{\varepsilon}_n$

whether dramatic increases in flow resistance (monitored simultaneously) are due to the stretching out of isolated molecules or of overlapping chains. Whilst confined to our specific technique for creating model elongational flow fields, we believe that our conclusions are pertinent to inhomogeneous flow fields with persistently extensional components in general.

EXPERIMENTAL

Solution preparation

Two partially hydrolysed polyacrylamide samples were used. The first one, manufactured by Aldrich, has a broad molecular-weight distribution and $\bar{M}_w > 5 \times 10^6$. The second one, manufactured by BDH, is also supposed to have a $\bar{M}_w > 5 \times 10^6$; however, we have evidence to suggest that this polymer possesses a higher mean molecular weight than the first (see first subsection in the discussion). The degree of hydrolysis of both samples was estimated by i.r. methods[32] and found to be $\sim 7\%$ for the Aldrich and $\sim 16\%$ for the BDH samples. Both $\bar{M}_w$ values are as quoted by the manufacturers.

The initial solvent used was freshly distilled and deionized water. Solutions were prepared with very slow stirring, allowing 48 h to ensure complete dissolution of the HPAA. All concentration units used are in w/w, and all the experiments were performed at room temperature (23°C).

The apparatus

Figure 7 shows a schematic diagram of the apparatus used to control and measure strain rate, observe birefringence and monitor the pressure drop across the jets.

A vacuum pump is used to suck the fluid through the jets in a controlled fashion. The flow rate is obtained from the pressure drop due to air flowing into the solution reservoir through a capillary (ΔP_1). Using this flow rate (Q) and the dimensions of the jets the strain rate can be to a first-order approximation calculated by[33]:

$$\dot{\varepsilon} = Q/Ad$$

where A is the area of the jet entrances and d the separation of the jets ($d = 1.2$ mm and the radius of both jets is 0.45 mm). The suction applied to the jets (ΔP_3) is monitored by a microcomputer, which drives a solenoid valve in order to uniformly increase the strain rate. While $\dot{\varepsilon}$ is being uniformly increased, the pressure drop across the jets (ΔP_2) is also recorded by the microcomputer.

The ΔP_2 vs. $\dot{\varepsilon}$ traces thus obtained showed a curvature even with pure solvent (see *Figure 10*), which originated from the Bernoulli effect due to convergent flow, an effect that can be corrected for analytically (see later). The slope of the corrected ΔP_2 vs. $\dot{\varepsilon}$ curve, $d(\Delta P_2)/d\dot{\varepsilon}$, then provides a quantity proportional to an elongational viscosity; this we have defined as the effective elongational viscosity η_e'[29]. This measure of extensional viscosity is a well defined function of macroscopic strain rate, but, because of the presence of a flow singularity, it must correspond to a combination of a wide range of fluid strains. Because of the way ΔP_2 is measured, there will also be a contribution to η_e' from Poiseuille flow inside the jets.

The optical system used to assess flow-induced birefringence consisted of a 2 m W polarized He–Ne laser focused by a condenser lens on the centre of the flow field. The birefringence patterns are observed between crossed polars utilizing a $\lambda/4$ plate as a Senarmont compensator. The polarized laser has an extinction ratio of 100:1, whilst the polarizer and analyser are Carl Zeiss components with extinction ratios of approximately 10^5:1.

Generally speaking, owing to the low intrinsic polarizability of the PAA chain, the birefringence patterns observed with HPAA are less intense than the

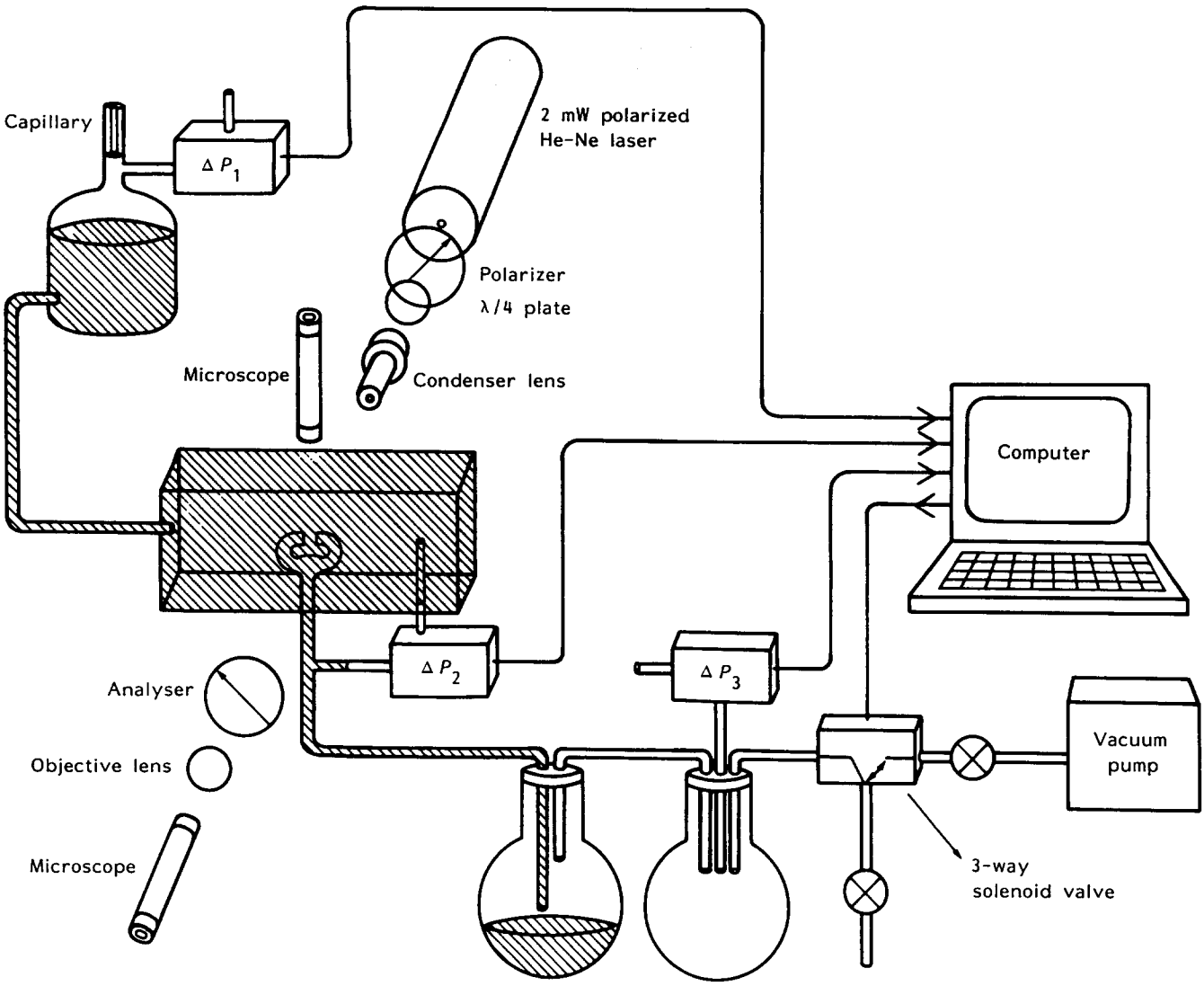

Figure 7 A schematic diagram of the apparatus used for measurement of extensional birefringence and flow resistance

ones previously observed for PEO and aPS at comparable solution concentrations. For this reason, photographic recording of clean images was very difficult and only a few successful photographs were obtained, and observations of birefringence effects below 400 ppm proved impossible.

Observations of light scattered at 90° from tracer particles were made on-line through a microscope, as shown in *Figure 7*. However, best results and maximum scattered intensity are obtained by removing the polarizer and $\lambda/4$ plate and substituting the condenser lens with a long-working-distance cylindrical lens. In this way the flow field is illuminated by a sheet of laser light of approximately 20 μm thickness.

RESULTS

The first set of experiments examine the behaviour of the HPAA polymers in the high ionic strength limit. We have used throughout 0.5 M NaCl solutions. Our experience showed that higher ionic strengths had no further effect (see below), a result in agreement with previous works, using similar polymers. This will be followed by the examination of the effects of ionic concentration below the high ionic strength limit, and by some experiments on the effect of pH.

HPAA in the high ionic strength limit—0.5 M NaCl solution

Molecular strain. As the strain rate is increased in a semi-dilute solution, the first observation is a narrow localized line corresponding to a region of highly stretched molecules. This is visible by both birefringence and scattered light observations. *Figure 8a* shows an example of (0.15%) of the birefringent line at $\dot{\varepsilon}_c$. *Figure 5c* is a photograph of the scattered light image (0.25%), again just above the critical coil–stretch transition. The use of light scattering to identify molecular strain is, in this context, a novel technique, here we use it simply to confirm strain patterns from a material that is very weakly birefringent. The results and interpretation of light scattering experiments *per se* will be discussed elsewhere[34].

At higher strain rates the line, observed both by birefringence and light scattering, progressively broadens and develops into a pipe at $\dot{\varepsilon}_p$ (see examples *Figure 8b* and *5d* respectively). The light scattering result (*Figure 5d*) corresponds to 90° scatter from a thin sheet ($\sim 20\,\mu$m) of laser light. The reality of the pipe structure, that is stretched molecules arranged around a cylinder, can be demonstrated by translating the jets across the beam. This reveals sections through the birefringent structure which clearly show a pipe-like cylindrical symmetry[34].

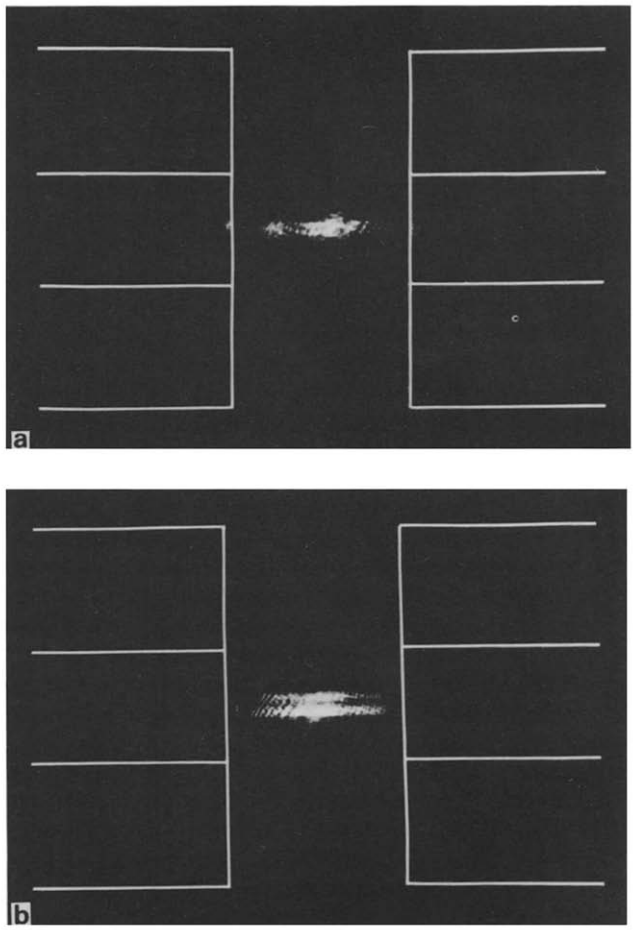

Figure 8 (a) A birefringent line between the jets for a 0.15% Aldrich HPAA/deionized water solution, $\dot{\epsilon} \approx 450\,s^{-1}$ ($\dot{\epsilon} > \dot{\epsilon}_c$). (b) A birefringent pipe between the jets for the same solution as *Figure 8a* but at $\dot{\epsilon} \approx 1000\,s^{-1}$ ($\dot{\epsilon} > \dot{\epsilon}_p$)

At even higher strain rates (beyond $\dot{\epsilon}_p$), the pipe structure breaks down and the flow becomes unstable as visualized by light scattered by tracer particles[29]. This signals the onset of the flare behaviour. The associated delocalization of birefringence (as in *Figure 6c*) can be observed but the signal is now very weak owing to the low polarizability of HPAA. This sequence of events for the collapsed HPAA molecule resembles closely the behaviour of other highly flexible molecules such as PEO and aPS[30].

All the above phenomena depend upon concentration and strain rate. *Figure 9* shows a 'phase diagram' illustrating the observed behaviour. At all concentrations and low strain rates the molecules exist in a coil-like state. At higher strain rates (above $\dot{\epsilon}_c$) the molecule undergoes a coil–stretch transition. The critical strain rate $\dot{\epsilon}_c$ is a slow function of concentration, reflecting the slightly increased viscosity of the solution. For concentration greater than 0.05% at higher strain rates ($\dot{\epsilon}_p$), the pipe appears, to be followed at strain rates greater than $\dot{\epsilon}_n$ by flare behaviour. The strain rates $\dot{\epsilon}_p$ and $\dot{\epsilon}_n$ are both strong functions of concentration, rapidly increasing to the maximum attainable strain rates as the concentration is reduced towards c_n^+.

Viscometry. Figure 10 illustrates the pressure drop across the jets (ΔP_2) as a function of strain rate in the coil–stretch and pipe regions of the phase diagram for a solution just above c_n^+ (0.06%). Curve A shows the behaviour of deionized water (as stated earlier the curvature is due to the Bernoulli effect, which can easily be subtracted—see for example *Figures 16* and *17*).

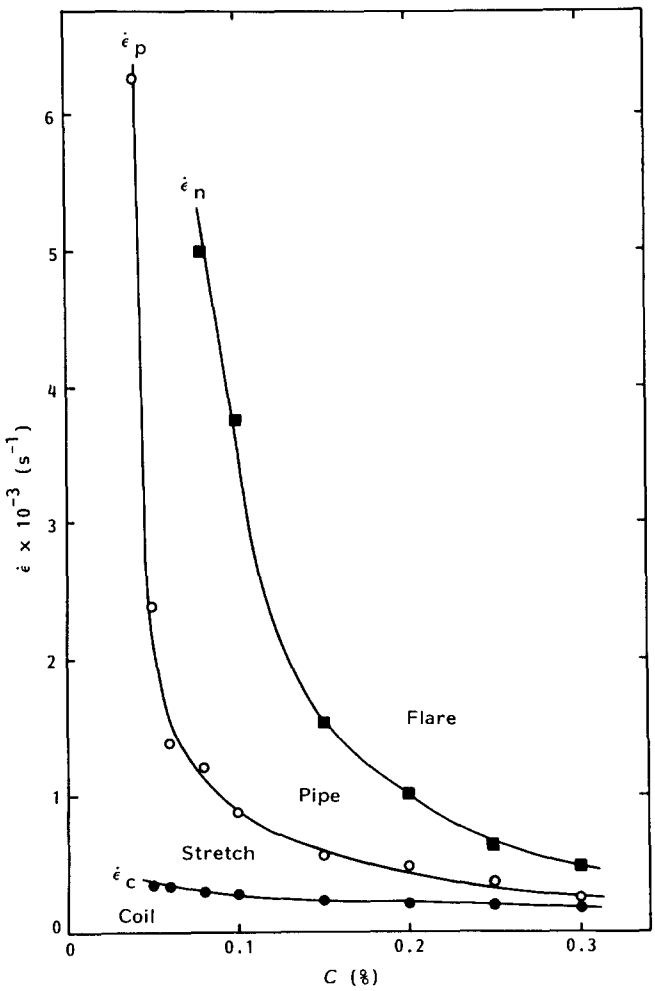

Figure 9 A 'phase diagram' of the development of connectivity as a function of strain rate and concentration: Aldrich HPAA ($\bar{M}_w > 5 \times 10^6$) in 0.5 M NaCl solutions

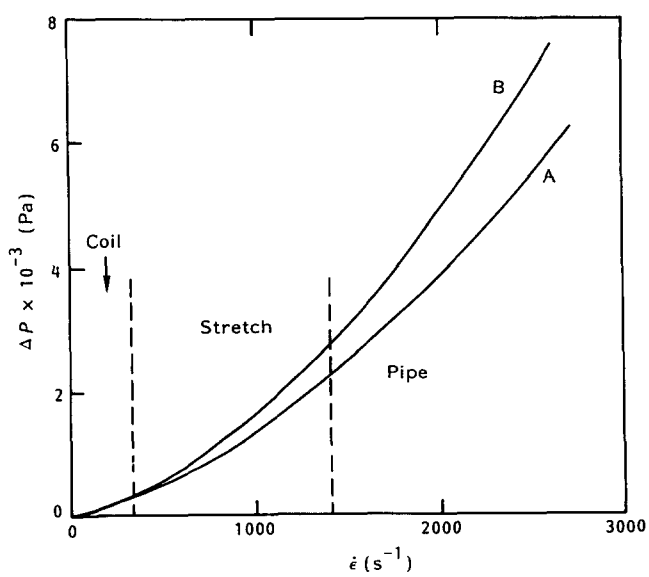

Figure 10 Pressure drop across the jets (ΔP_2 in *Figure 7*) *versus* $\dot{\epsilon}$ for: A, deionized water; B, 0.06% Aldrich HPAA in 0.5 M NaCl solution

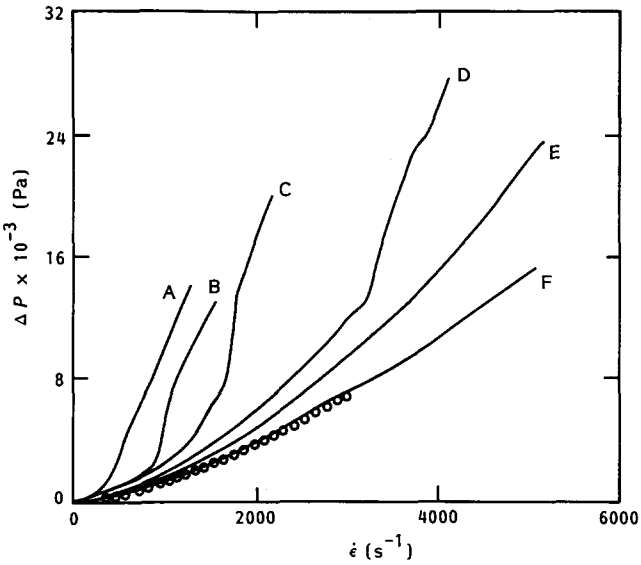

Figure 11 Pressure drop across the jets *versus* $\dot{\epsilon}$ for the Aldrich HPAA in 0.5 M NaCl solutions at: A, 0.3%; B, 0.2%; C, 0.15%; D, 0.1%; E, 0.06%; F, 0.01%. Open circles are for deionized water

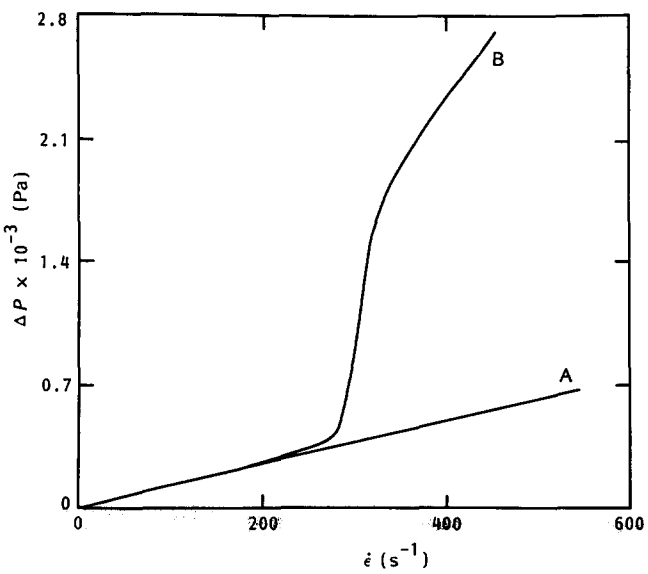

Figure 12 Pressure drop across the jets *versus* $\dot{\epsilon}$ for: A, deionized water; B, 0.02% BDH HPAA ($\bar{M}_w > 5 \times 10^6$) in 0.5 M NaCl solution. Both curves are corrected for the Bernoulli effect

Compared to water the polymer solution (curve B) exhibits a modest increase ($\sim 10\%$) in flow resistance corresponding to the stretch and pipe regions of the phase diagram.

Figure 11 explores the strain-rate dependence of ΔP_2 for the Aldrich HPAA (0.5 M NaCl) as a function of concentration, and extending the strain-rate range to include the flare region of the phase diagram. At each concentration when the strain rate exceeds $\dot{\epsilon}_n$ (i.e. the system flares), there is a corresponding enormous increase in flow resistance compared to deionized water (open circles) and to polymer solutions below c_n^+ (curve F).

Parallel effects are seen in 0.5 M NaCl solutions of the BDH HPAA polymer, except that the effects are shifted to lower strain rates and concentrations—an effect previously ascribed to higher molecular weight. *Figure 12* gives an example of a curve of flow resistance *versus* strain rate corrected for the Bernoulli effect. The strain rate $\dot{\epsilon}_n$ occurs at about 280 s^{-1}, as evidenced by the observation of flow instabilities. Beyond $\dot{\epsilon}_n$, there occurs a dramatic increase in flow resistance associated with the flare condition.

The behaviour of HPAA as a function of ionic environment

The behaviour of HPAA solutions when made in deionized water are strikingly different. For this purpose we use the more highly hydrolysed BDH polymer, as here the effects of ionic environment are more pronounced. *Figure 13* presents the flow-resistance data as a function of strain rate and ionic strength. Consider first the case of the salt-free solution. In contrast to what was observed for high ionic strength above, here the flow resistance of the polymer solution (curve B) is much higher than that of deionized water alone (curve A) from the lowest strain rates (i.e. there is no apparent criticality in the onset of flow resistance). Also the flow is always unstable, a laminar flow field as in *Figure 5b* never being observed even at the lowest strain rates. Re-runs of curve B exhibit progressive reduction in pressure drop, indicative of degradation (see below). All these observations suggest that this solution is always in the flare state; indeed in HPAA concentration above 400 ppm, this behaviour could be visually identified as flare from birefringence observations.

In the presence of salt, the flow resistance enhancement occurs only above a critical strain rate, which progressively increases with the salt concentration. Beyond 0.3 M no further changes were observed (curves C–G in *Figure 13*). *Figure 14* shows another example of the same phenomenon at higher concentration of HPAA in the limits of deionized water and 0.5 M salt solution. *Figure 15* presents an effective elongational viscosity derived from the curves in *Figure 14*, after correction for the Bernoulli effect.

This flare effect in deionized water can persist to extremely low concentrations. *Figure 16* shows the flow resistance *versus* strain rate for a 4 ppm solution of BDH HPAA, which still exhibits a marked departure from

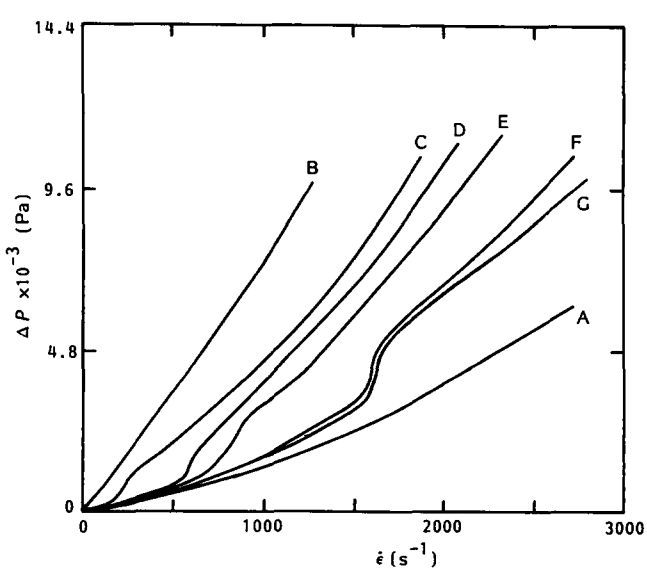

Figure 13 Pressure drop across the jets *versus* $\dot{\epsilon}$ for 0.005% BDH HPAA in NaCl solution of: B, 0 M; C, 0.05 M; D, 0.1 M; E, 0.15 M; F, 0.3 M; G, 0.5 M; curve A is for deionized water

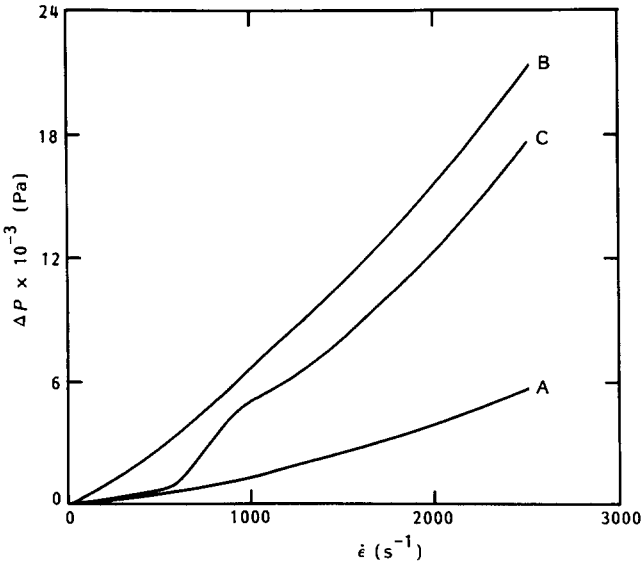

Figure 14 Pressure drop across the jets *versus* $\dot{\varepsilon}$ for: A, deionized water; B, 0.01% BDH HPAA/deionized water solution; C, 0.01% BDH HPAA in 0.5 M NaCl solution

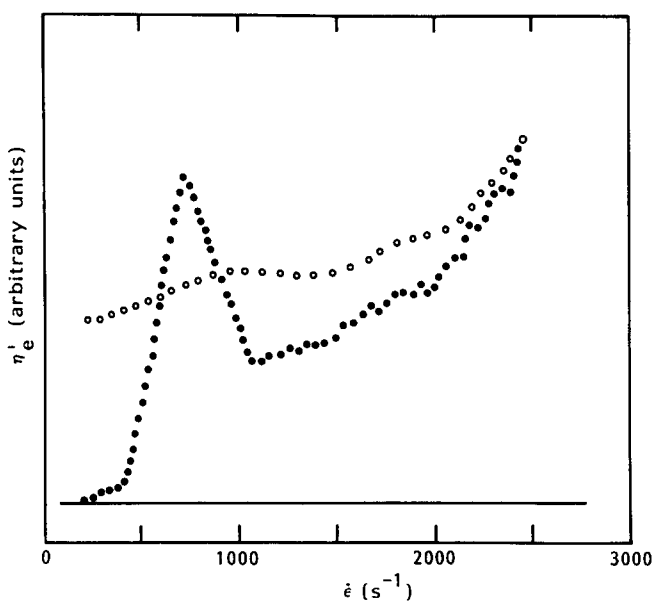

Figure 15 Plot of η'_e *versus* $\dot{\varepsilon}$ for: ○, 0.01% BDH HPAA/deionized water solution; ●, 0.01% BDH HPAA in 0.5 M NaCl solution; ———, deionized water

deionized water behaviour (curve A). In 0.5 M NaCl, however, the solution is indistinguishable from pure water (curves B and open circles respectively).

Figure 17 presents the same data, but corrected for the Bernoulli effect, shown here to illustrate the magnitude of the correction as mentioned in the Experimental section.

pH and degradation effects

The behaviour of the HPAA molecule is sensitive not only to the presence of salt but also to the solution pH.

As prepared in deionized water all the solutions are slightly acid (pH 6). The addition of 0.1% by volume glacial acetic acid reduces the pH to 3.5. The effect of this pH reduction on the measured flow resistance is very similar to the effect of excess salt. *Figure 18* (curve A) shows the Aldrich HPAA in deionized water. After the addition of 0.1% glacial acetic acid (curve B—open circles) the polymer behaviour is indistinguishable from water.

Figure 19 shows the BDH polymer in deionized water (curve B) and with the addition of acetic acid (curve C). This polymer, however, will flare in the acid environment beyond 400 s^{-1}, as it did in the excess salt environment (*Figure 12*).

Curves C–F of *Figure 19* illustrate successive runs of the same polymer solution. The progressive shift of $\dot{\varepsilon}_n$ to higher values and progressive reduction in the effectiveness of flow resistance are indicative of degradation. This degradation only occurs whilst the solution is flowing in the flare state ($\dot{\varepsilon} > \dot{\varepsilon}_n$), a behaviour that is essentially the same as previously reported for PEO[29].

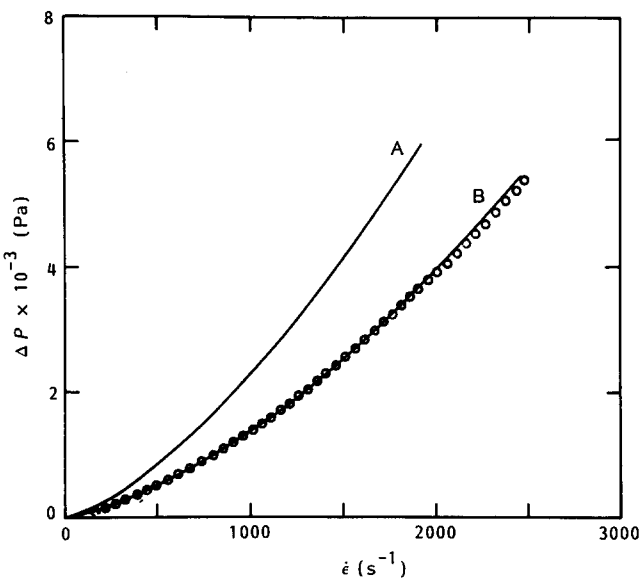

Figure 16 Pressure drop across the jets *versus* $\dot{\varepsilon}$ for: A, 0.0004% BDH HPAA/deionized water solution; B, 0.0004% BDH HPAA in 0.5 M NaCl solution; ○, deionized water

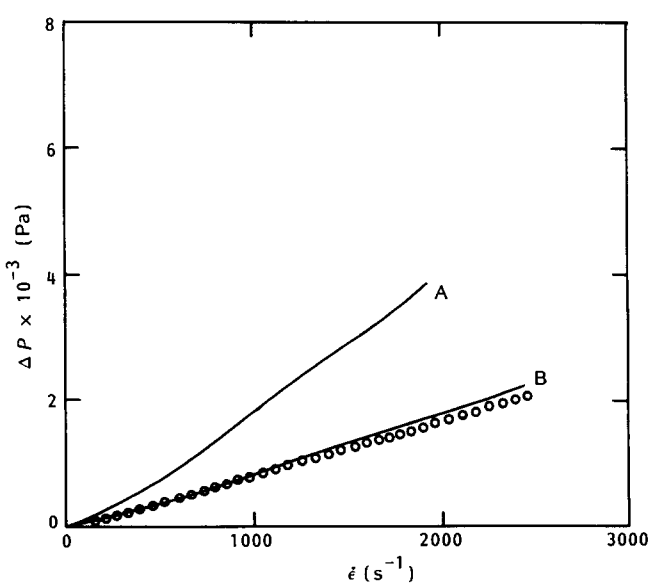

Figure 17 Same curves as for *Figure 16* but corrected for the Bernoulli effect

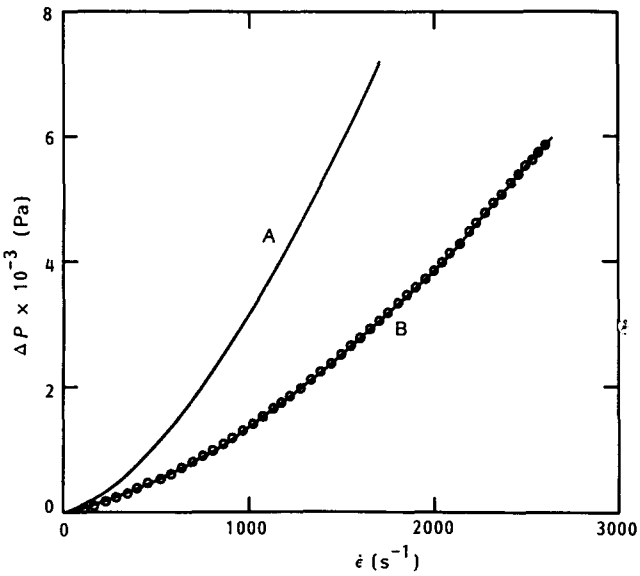

Figure 18 Pressure drop across the jets *versus* $\dot{\epsilon}$ for: A, 0.01% Aldrich HPAA/deionized water solution (pH = 6); B, 0.01% Aldrich HPAA in 0.1% glacial acetic acid solution (pH = 3.5); ○, deionized water

DISCUSSION

The HPAA molecule can be considered as a polyelectrolyte. As we have seen, in the presence of excess counterions, the polyelectrolyte behaviour is masked, and the molecule behaves as a flexible coil, the conformation of which depends on solvent quality, and we can rationalize the extensional flow behaviour by comparison with non-ionic flexible molecules. In deionized water the coil is expected to be highly expanded[35], and as we have seen this dramatically affects its extensional flow behaviour.

HPAA in sodium chloride solutions

The phase diagram (*Figure 9*) of Aldrich HPAA summarizes the visual observations as a function of strain rate and concentration. Such curves bear a strong resemblance to those of non-ionic flexible polymers such as PEO and aPS[29,30]. As previously observed, both the pipe and flare behaviours are strongly concentration-dependent; below a critical concentration c_n^+ ($\sim 0.05\%$ in *Figure 9*), only a coil–stretch transition is observed. As stated earlier this is considerably below the values typically taken for conventional c^* based upon packing of molecules of radius R_g.

In accordance with previous results this leads us to the interpretation of the pipe and flare as manifestations of the onset of connectivity, due to a transient weakly overlapping network which is only mechanically effective on very short timescales such as realized by these experiments[25,30].

The elongational viscometry apparatus (*Figure 7*) enables the flow resistance to be measured simultaneously as the strain patterns of *Figure 9* are observed. We can thus equate non-Newtonian viscosity effects directly with the behaviour of the molecules. *Figure 10* shows the influence of the coil–stretch and stretch–pipe transitions (as identified visually) on the flow resistance. We observe only a modest increase in flow resistance compared to water.

Extending the viscometry to higher concentrations and strain rates considerably beyond the stretch–pipe transition (*Figure 11*), dramatic non-Newtonian dilatant behaviour sets in above c_n^+, the corresponding $\dot{\epsilon}_n$ being a decreasing function of concentration; below the critical concentration of the phase diagram (*Figure 9*) no additional flow resistance compared to water is observed (*Figure 11*, curve F).

On the basis of delocalization of birefringence, light scattering and the breakdown of stagnation point flow (see Figure 6 in ref. 29), we can unambiguously associate the non-Newtonian region with the flare behaviour (i.e. transient network effect). Further, flow in this region is always associated with polymer degradation (*Figure 19*), as previously observed in other flexible polymers[29,30].

Figure 12 shows viscometry of the second material (BDH), and demonstrates the considerable magnitude of the increase of flow resistance with respect to water beyond $\dot{\epsilon}_n$. The concentration here (0.02%) is considerably below c^* for the Aldrich polymer. Since we are now comparing the two polymers in the limit of high counterion concentration, we attribute the difference to the BDH polymer containing more high-molecular-weight species. As stated earlier it proved impossible to observe birefringence in HPAA at such low concentrations. However, the viscometry, the criticality of the effect, the breakdown of the flow field and the progressive degradation of the chains leave no doubt that the effect is associated with transient network behaviour beyond $\dot{\epsilon}_n$.

HPAA in pore flow

The above findings lead us to a new interpretation of results from porous media and capillary entrance flow. As outlined in the Introduction, strong non-Newtonian effects have previously been attributed to the increase in extensional viscosity associated with the coil–stretch transition, occurring when the strain rate exceeds the reciprocal of the lowest-order conformational relaxation time.

There are already two problems with this approach.

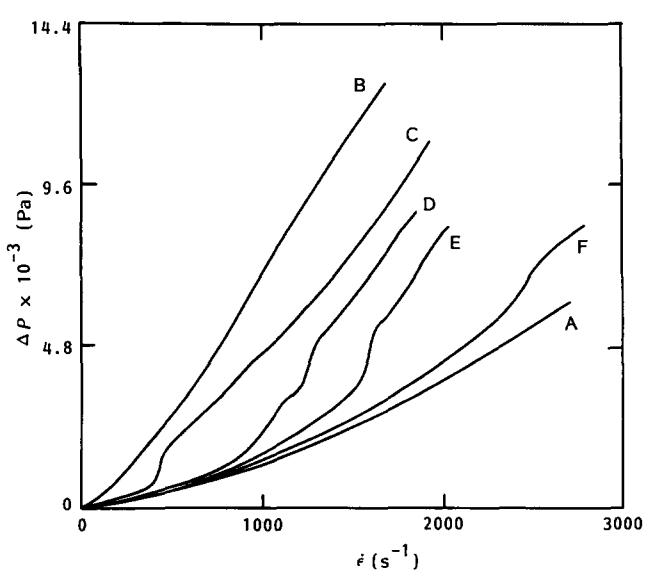

Figure 19 Pressure drop across the jets *versus* $\dot{\epsilon}$ for: A, deionized water; B, 0.02% BDH HPAA/deionized water solution; C, as B after addition of 0.1% glacial acetic acid; D, as C after two runs; E, as C after four runs; F, as C after six runs

First, these polymers are invariably highly polydisperse, which would result in a wide range of relaxation times ($\tau \propto M^{1.5}$); further, the effective pore radius distribution is large[14]. Together these effects should produce a rather gradual onset of increased flow resistance when $\dot{\varepsilon}$ increases beyond $\dot{\varepsilon}_c$, which is not the case, the observed onset of flow resistance enhancement being very sudden (see *Figures 2–4*).

Secondly, the strain required to stretch out a high-molecular-weight polymer fully is typically 200 times[6]. In capillary entrance experiments, however, the fluid strain is often quite small (<25 times[12]). This does not apparently prevent the observation of the phenomenon of flow resistance enhancement. We believe that the primary effect observed corresponds to the transient network flare behaviour. The evidence is as follows.

The visually observed coil–stretch transition *does not* correspond to pronounced viscosity effects such as seen in refs. 1–3 and 10–15. The latter are seen in our experiments but are always associated with the flare.

The degradation that is always observed in the flare state (but not in the stretch state) parallels that of *Figure 4*, and has been reported to occur in all cases where enhanced flow resistance is encountered[15]. Further, degradation is not restricted to the largest molecules (as would be the expectation for stretched molecules in isolation at $\dot{\varepsilon} \gg \dot{\varepsilon}_c$[22]) but occurs in all molecular-weight ranges that fulfil the condition of adequate strain rate[15].

The flow resistance as measured in our experiments may increase apparently indefinitely beyond $\dot{\varepsilon}_n$ (see *Figures 11–14*). This is in contrast to the effects seen in pore flow experiments (typically *Figure 3*) where the flow resistance levels off, and may even reduce at high strain rates. We associate our continuing rise with always new, previously unstretched molecules entering the flow field, which are then broken for the first time by the flow.

Our results suggest that the onset strain rate of flare instability (and associated flow resistance) remains a strong function of concentration. Kulicke and Haas, however, invoke as evidence that the effect is due to the coil–stretch transition, the contention that for a given molecular weight, increasing the concentration below a certain limit does not affect the onset behaviour, but increases the maximum flow resistance. If, however, one extracts the onset Reynolds number (*Re*) as shown in *Figure 4*, for each curve of *Figure 3* two features emerge: first, no concentration can be identified below which the onset Reynolds number is independent of concentration; and secondly, the magnitude of the effect is not proportional to the polymer concentration, both of which would be anticipated for the dilute regime coil–stretch transition.

The dependence of our flow resistance anomalies for HPAA upon salt concentration (*Figure 13*) is strikingly similar to the salt dependence of pore flow viscosity enhancement (*Figure 2*). The critical onset strain rate from our experiments varies in the same way as the critical onset Reynolds number in pore flow. In both experiments no further dependence on salt concentration is observed beyond 0.5 M. Further, in deionized water, both experiments show non-Newtonian behaviour (in our case identifiable as flare) even at the lowest flow rates (for further discussion of pure water results see below).

As mentioned above, the criticality of onset of flow resistance enhancement appears incompatible with the known polydispersity if interpreted on the basis of the coil–stretch transition. Indeed, in our experiments the coil–stretch transition as identified by birefringence occurs over a wide range of strain rates, consistent with the wide range of molecular weights present in the polydisperse material (*Figure 10*). The transition to network behaviour (flare), however, is always sharply critical (*Figure 11*). This might be expected for the development of long-range connectivity, on the basis of percolation theory[36].

The interpretation of the dilatant behaviour as a network deformation phenomenon avoids the requirement for large accumulated molecular strains; this also accounts for the delocalization of birefringence in the flare state (*Figure 6c*) where a stagnation point is no longer present to accumulate large strains. Thus we can explain large non-Newtonian effects at relatively low strains in, for instance, capillary entrance experiments[12].

Solutions without salt

In deionized solutions, as we have seen, the flare flow instability is seen from the lowest strain rates and extends to much lower concentrations (*Figures 13–17*). The effects of counterions (*Figure 13*) and pH (*Figure 18*) confirm that this is due to polyelectrolytic behaviour in the HPAA[10]. This effect is particularly pronounced with the BDH polymer since its degree of hydrolysis is 16% compared to 7% for the Aldrich polymer.

This has been previously interpreted as an effect due to coil expansion, which in turn increases the viscosity and relaxation time of the coil[10,13,37]. Such a dramatic effect of coil expansion upon the relaxation time (in dilute solution) has been identified for poly(styrene sulphonate) (a closely monodisperse polyelectrolyte) in pure extensional flow[38].

The dramatic coil expansion, however, would of course result in molecular overlap at much lower concentrations, which is consistent with our interpretation of the flare-type behaviour as a network effect. Indeed, light scattering experiments on polyelectrolytes are known to be difficult, hardly ever yielding scattering that can be attributed to the isolated coil[39].

Figure 14 shows the behaviour of a deionized solution of BDH HPAA (curve B). On addition of salt (curve C) the behaviour at low strain rates becomes indistinguishable from water (curve A), owing to contraction of the coil resulting from screening of the periodic charges. If the concentration is high enough, as in C of *Figure 14*, then the behaviour of semi-dilute solutions with salt is replicated, i.e. network behaviour can be observed beyond $\dot{\varepsilon}_n$ (see, for comparison, B of *Figure 12*). For concentrations below the value of c_n^+, appropriate for excess NaCl, no subsequent flare state was observed up to the highest strain rates.

The effective elongational viscosity corresponding to *Figure 14* is depicted in *Figure 15*. The horizontal line for the water corresponds to a constant Newtonian-type behaviour. The solution in deionized water (open circles) shows a greatly increased low-strain-rate elongational viscosity gradually increasing with strain rate, corresponding to flare-type behaviour from the lowest strain rates. For the 0.5 M solution (filled circles) the low-strain-rate viscosity is indistinguishable from water. Beyond $500\,s^{-1}$, however, it becomes strongly non-Newtonian, rising through a maximum then

progressively increasing towards the value of the solution in deionized water.

The peak in η_e' is known from birefringence, flow field and light scattering observations to correspond to the highest $\dot{\varepsilon}$ for which a stagnation-point-type flow is maintained. At higher strain rates the solution flares, and the effective elongational viscosity drops. We should recall that η_e' is here defined as the instantaneous gradient of the flow resistance, so that flow resistance is still high, even though η_e' may drop. We see this fall in η_e' as due to the loss of the stagnation point, which means that the solution no longer needs to achieve extremely high strains during the opposed jet flow. A peak in the effective viscosity (the gradient of flow resistance *versus* strain rate) is also implicit in earlier data (*Figures 1–4*). This is not the expectation for a coil–stretch transition in truly dilute solution, a topic upon which we will report elsewhere[34].

Figures 16 and *17* illustrate that large degrees of viscosity enhancement are observable to remarkably low concentrations for the BDH polymer in deionized solutions (4 ppm). It is clear, however, that the effects observed are much greater than we would anticipate due to the isolated molecule. We suspect that this polymer has very high molecular weight and is known to have a high degree of hydrolysis, which results in an extremely expanded coil in solution.

It might be that a genuine network exists even at such low concentrations (c^* for a rod-like HPAA of $\bar{M}_w = 5 \times 10^6$ would be ~ 0.1 ppm), but it is also possible that the effect is due to molecular aggregation without complete network development[16,17], or to long-range cooperative effects arising from the electrolytic nature of the chain. This is a topic of current investigation.

CONCLUSIONS

In this paper we have presented a new technique, based upon our idealized extensional flow systems, whereby we can measure directly the macroscopic elongational viscosity and simultaneously observe the development of molecular extension. We have observed remarkable viscosity enhancement at high strain rates. Such phenomena have been shown to be due to the onset of flow instabilities associated with the development of transient networks.

We believe that many anomalous non-Newtonian effects reported previously in flows that contain appreciable elongational components parallel these phenomena, particularly pore flow, and are themselves due to the existence of transient networks.

ACKNOWLEDGEMENT

We are pleased to acknowledge the support of the Venture Research Unit of BP International during the course of this research.

REFERENCES

1 Dauben, D. L. and Menzie, D. E. *J. Petrolm. Technol.* 1967, **240**, 1065; MacWilliams, D. C., Rogers, J. H. and West, T. J. *Polym. Sci. Technol.* 1973, **2**, 105
2 Marshall, R. J. and Metzner, A. N. *Ind. Eng. Chem. Fundam.* 1967, **6**, 393
3 James, D. F. and McLaren, D. R. *J. Fluid Mech.* 1975, **70**, 733
4 de Gennes, P. G. *J. Chem. Phys.* 1974, **60**, 5030
5 Hinch, E. J. *Phys. Fluids* 1977, **20**, S22
6 Bird, R. B., Hassager, O., Armstrong, R. C. and Curtiss, C. F. 'Dynamics of Polymeric Liquids', Wiley, New York, Vol. 2, 1977
7 Christiansen, R. L. and Bird, R. B. *J. Non-Newtonian Fluid Mech.* 1977/78, **3**, 161
8 Bird, R. B., Dotson, P. J. and Johnson, N. L. *J. Non-Newtonian Fluid Mech.* 1980, **7**, 213
9 Warner, H. R. *Ind. Eng. Chem. Fundam.* 1972, **11**, 379
10 Ouibrahim, A. and Fruman, D. H. *J. Non-Newtonian Fluid Mech.* 1980, **7**, 315
11 Moan, M., Chauveteau, G. and Ghoniem, S. *J. Non-Newtonian Fluid Mech.* 1979, **5**, 463
12 Chauveteau, G., Moan, M. and Magueur, A. *J. Non-Newtonian Fluid Mech.* 1984, **16**, 315
13 Durst, F., Haas, R. and Kaczmar, B. U. *J. Appl. Polym. Sci.* 1981, **26**, 3125
14 Kulicke, W. M. and Haas, R. *Ind. Eng. Chem. Fundam.* 1984, **23**, 308; Haas, R. and Kulicke, W. M. *Ind. Eng. Chem. Fundam.* 1984, **23**, 316
15 Haas, R. and Kulicke, W. M. 1985 in Proc. IUTAM Symp., Essen, 26–28 June 1984, (Ed. B. Gampert), Springer, Berlin, p. 119
16 Layec-Raphalen, M. N. and Wolff, C. 1985 in Proc. IUTAM Symp., Essen, 26–28 June 1984, (Ed. B. Gampert), Springer, Berlin, p. 143
17 Ferguson, J., Hudson, N. E., Warren, B. C. H. and Tomutarian, A. *Nature* 1987, **325**, 234
18 Keller, A. and Odell, J. A. *Colloid Polym. Sci.* 1985, **263**, 181
19 Frank, F. C. and Mackley, M. R. *J. Polym. Sci., Polym. Phys. Edn.* 1976, **14**, 1121
20 Pope, D. P. and Keller, A. *Colloid Polym. Sci.* 1978, **256**, 751
21 Miles, M. J. and Keller, A. *Polymer* 1980, **21**, 1295
22 Odell, J. A. and Keller, A. *J. Polym. Sci., Polym. Phys. Edn.* 1986, **24**, 1889
23 Odell, J. A. *J. Polym. Sci., Polym. Phys. Edn.* submitted
24 Farrell, C. J., Keller, A., Miles, M. J. and Pope, D. P. *Polymer* 1980, **21**, 129
25 Odell, J. A., Keller, A. and Miles, M. J. *Polymer* 1985, **26**, 1219
26 Zimm, B. H. *J. Chem. Phys.* 1956, **24**, 269
27 Rabin, Y. *J. Polym. Sci. Lett.* 1985, **23**, 11
28 Odell, J. A., Keller, A. and Miles, M. J. *Polym. Commun.* 1983, **24**, 7
29 Chow, A., Keller, A., Müller, A. J. and Odell, J. A. *Macromolecules* 1988, **21**, 250
30 Keller, A., Müller, A. J. and Odell, J. A. *Prog. Colloid Polym. Sci.* 1987, (in press)
31 Aharoni, S. M. *J. Macromol. Sci.–Phys.* (*B*) 1978, **15**(3), 347
32 Guerrero, S. J., Boldarino, P. and Zurimendi, J. A. *J. Polym. Sci., Polym. Phys. Edn.* 1985, **30**, 955
33 Mackley, M. R. and Keller, A. *Phil. Trans. R. Soc. Lond.* (*A*) 1975, **278**, 29
34 Keller, A., Müller, A. J. and Odell, J. A., to be published
35 Oozawa, F. 'Polyelectrolytes', Marcel Dekker, New York, 1971
36 Staufer, D., Coniglio, A. and Adam, M. *Adv. Polym. Sci.* 1982, **44**, 103
37 Kuliche, W.-M. and Klein, J. 1985, in Proc. IUTAM Symp., Essen, 26–28 June 1984, (Ed. B. Gampert), Springer, Berlin, p. 143
38 Miles, M. J., Tanaka, K. and Keller, A. *Polymer* 1983, **24**, 1081
39 Morawetz, H. 'Macromolecules in Solution', 2nd Edn., Wiley Interscience, New York, 1975